Attosecond transient absorption spectroscopy of helium above the N=2 ionization threshold

C. L. M. Petersson, Luca Argenti, and Fernando Martín

Attosecond transient absorption spectroscopy of Helium above the $N = 2$ ionization threshold

C. L. M. Petersson,[1] Luca Argenti,[1, 2] and Fernando Martín[1, 3, 4, *]

[1]*Departamento de Química, Módulo 13, Universidad Autónoma de Madrid, 28049, Madrid, Spain*
[2]*Department of Physics & CREOL, University of Central Florida, Florida 32816, USA*
[3]*Instituto Madrileño de Estudios Avanzados en Nanociencias (IMDEA-Nanociencia), 28049 Madrid, Spain*
[4]*Condensed Matter Physics Center (IFIMAC), Universidad Autónoma de Madrid, 28049 Madrid, Spain*
(Dated: June 14, 2017)

Attosecond transient absorption spectroscopy (ATAS) allows for the study of electron dynamics in atoms and molecules with attosecond time resolution. Previous works reported in the literature have made use of ATAS to image and control such dynamics in the single-channel ionization continuum of helium, in particular, in the vicinity of the doubly excited autoionizing states lying between the $N = 1$ and $N = 2$ thresholds. In this work, we have extended these studies to autoionizing states lying above the $N = 2$ threshold, where several ionization channels are open. From an accurate solution of the time-dependent Schrödinger equation, we predict the appearance of pronounced one-photon beatings between the $3snp$ states and the adjacent $^1S^e$ and $^1D^e$ resonances, as well as, more suprisingly, two-photon beatings between the $3s3p$ doubly excited state and the $^1P^o$ *non resonant* continuum. Both effects lead to a significant distortion of the $3snp$ Fano profiles and to a strong variation of these profiles with the pump-probe delay, thus demonstrating control of the corresponding multi-channel two-electron correlated wave packets, in the same way as reported for resonances lying below the $N = 2$ threshold.

I. INTRODUCTION

Attosecond transient absorption spectroscopy (ATAS) [3] has become one of the reference tools to investigate electron dynamics in atoms and molecules at their natural time scale [3–5], and in particular to visualize and control electron wave-packet dynamics induced by attosecond light sources. To name a few applications, ATAS has been employed to monitor hole alignment in neon [6] and to trace the ultrafast dynamics resulting from the coherent superpositions of valence-hole excited states in krypton [3, 7], of singly-excited bound states in neon [5, 8] and helium [9–13], and of doubly-excited states in helium [2, 4]. ATAS is a pump-probe technique in which the pulse sequence comprises a weak extreme ultraviolet (XUV) attosecond pulse in combination with an additional control pulse, typically in the visible or infrared energy range. The spectrum of the XUV pulse transmitted through a sample is recorded as a function of the time delay between the XUV and the control pulse. With ATAS it is easier to achieve high energy resolution than with experimental techniques based on the detection of photo-electrons or ions [14, 15]. This is because photons are more easily collected from the interaction region without the subsequent distortions experienced by charged massive particles on their way to the detector [16]. Furthermore, transient absorption spectra are mostly sensitive to the population of states with a strong dipolar coupling to the ground starte. While this feature limits the dynamics ATAS can monitor, it also makes the spectrum much easier to interpret. The practical advantage of transient absorption spectroscopies over photoelectron or photo-ion spectroscopies is even more pronounced for condensed samples. Photoelectrons emitted from the bulk of a solid, or from a molecule in solution, experience multiple scattering events before reaching the detector, which deteriorate their spectral and coherence properties. Light, on the other hand, can propagate for longer distances before appreciably interacting with the matrix medium. This is particularly the case for molecules in aqueous solutions when their absorption spectrum is measured in the water window, i.e., the energy range between carbon and oxygen K edge, where water is virtually transparent. ATAS is also easier to simulate than photoelectron spectra. While to compute the latter it is necessary to propagate charged particles to the asymptotic region, absorption spectra require to accurately describe the electronic wave function only in a small spatial region near the origin, where the ground state does not vanish.

In the version of ATAS examined in the present work, the weak attosecond XUV pulse populates excited bound or continuum electronic states of the target atom or molecule, which in turn give rise to an oscillating dipole moment whose radiation interferes with the same XUV pulse that promoted the transition. The XUV pulse, therefore, acts both as a pump and a probe of the ultrafast dynamics in the target. If the sample is sufficiently thin, so that macroscopic propagation effects can be neglected, the variation in the XUV spectrum reflects the XUV dipolar response of an isolated target atom or molecules across time. A few-cycle visible (VIS) control pulse, having a known time delay with respect to the XUV pulse, can alter the dipolar response in two ways. If the XUV and the VIS pulse overlap, the initial XUV

one-photon transition takes place between dressed rather than field-free states. If the VIS pulse arrives after the XUV pulse, it transfers population between the excited states and changes their relative phases, thus altering the time evolution of the electronic wave packet, and in turn that of the dipole oscillations with the ground state as well. The absorption spectrum encodes full information on the dipole response of the system. By varying the time delay t_d between the XUV and VIS pulses, the signature of coherent electron excitations, i.e., of the generated electron wave packet, emerges. The time evolution of such an electron wave packet can be controlled by altering the relative phase of its components. In particular, ATAS has successfully been used to investigate the dynamics of the lowest autoionizing states in He as well as to control autoionization itself [17]. Indeed, a change in the interference between direct and resonant ionization leads to a modulation of the asymmetry of the resonant profiles, which is clearly visible in the transient absorption spectrum [17–19].

This principle has recently been demonstrated in the case of a two-electron wave packet formed by a coherent superposition of the $sp_{2,n}^+$ $^1P^o$ doubly excited states (DES) in He [4, 17]. The experiment revealed the Autler–Townes (AT) splitting of the $2s2p$ state, the lowest state in the $^1P^o$ autoionizing series, due to the coupling with the $2p^2$ ^1S state [4], as well as the inversion of the Fano profile associated with the higher terms of the $sp_{2,n}^+$ series as a function of both the pump-probe time delay and the intensity of the VIS dressing field [17]. So far, ATAS studies of electronic coherence in helium have been restricted to the region below the $N = 2$ threshold, where ionization can only result in a cation in its ground state, $He^+(1s)$. In this paper we explore the region above the $N = 2$ threshold, where, in addition to $He^+(1s)$, ionization can lead to excited $He^+(2s)$ and $He^+(2p)$ ions. Our aim is to extend the studies of resonant features in transient-absorption spectra from the single channel to the multichannel case, which is the usual scenario in more complex atoms and molecules.

For this, we have numerically solved the time-dependent Schrödinger equation (TDSE) for the helium atom in the presence of a weak isolated attosecond XUV pulse, with an intensity of 10^{11} W/cm^2, a central frequency of 2.5 a.u. (68 eV) and a spectral FWHM of 0.18 a.u., in combination with a moderately intense VIS pulse, with an intensity of 4×10^{12} W/cm^2, a central wavelength of 798nm, corresponding to a frequency of 0.057117 a.u. (1.5 eV), and a spectral FWHM of 0.025 a.u. The XUV pulse can directly populate the doubly excited states of He lying above the $N = 2$ threshold by absorption of just a single photon (see Figure 1). The VIS pulse allows us, e.g., to induce the transitions depicted in Figure 1. The laser parameters used in this work are similar to those employed by Ott et $al.$ [4, 17] in their experimental study of doubly excited states below the $N = 2$ threshold.

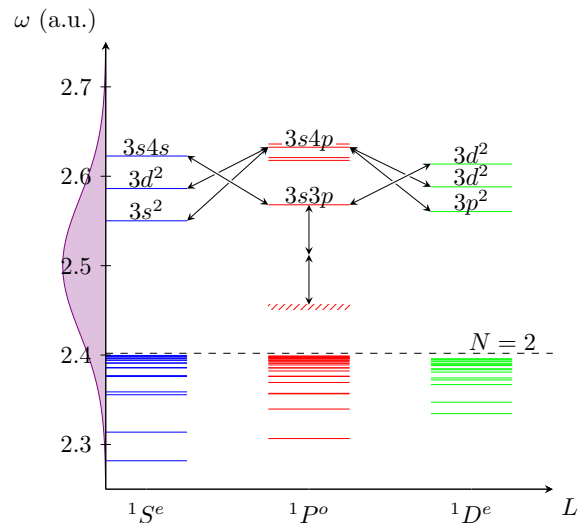The resonant features in the ATAS spectrum above the $N = 2$ threshold are less pronounced than in the

FIG. 1. A diagram of $^1S^e$, $^1P^o$, and $^1D^e$ helium energy levels below and above the $N = 2$ threshold [20–22]. The P continuum between the $N = 2$ threshold and the $3s3p$ doubly excited state is illustrated with diagonal stripes. The $N = 2$ threshold is indicated by a black, dashed line. The frequency distribution of the XUV used to populate the states, shown to the left, is centered at 2.5 a.u. and has a FWHM of 0.18 a.u.. Likely transitions due to the VIS, which has a central frequency of 0.057 a.u., are illustrated using arrows.

single-channel case: the resonances are broader (more decay channels available) and less bright than those below the $N = 2$ threshold, in line with the autoionization and dipole-transition propensity rules characteristic of two-electron atoms [23]. Nevertheless, we show that, with the present choice of laser parameters, we are still able to induce sizable resonant one-photon transitions between the $3snp$ $^1P^o$ doubly excited states and the $3l3l'$ $^1S^e$ and $^1D^e$ ones. More interestingly, we also observe two-photon beatings associated with the bound-continuum transition from the $3s3p$ $^1P^o$ DES to the non resonant $^1P^o$ multichannel continuum lying just above $N = 2$, thus leading to the formation of a multichannel two-electron correlated wave packet. Both effects lead to a significant distortion of the $3snp$ Fano profiles and to a strong variation of these profiles with the pump-probe delay, thus demonstrating control of multi-channel resonant profiles in the same way as reported for resonances lying below the $N = 2$ threshold [17].

The paper is organized as follows. In section II we briefly describe our theoretical method and in section III we present the calculated ATAS spectrum and a two-dimensional analysis which reveals the main beatings of the formed electron wave packet. Section IV summarizes the main conclusions of our study. In the following, we will use atomic units unless otherwise specified.

II. THEORETICAL MODEL

The transient spectrum in the velocity gauge, σ, is given by the expression

$$\sigma(\omega) = -\frac{4\pi}{\omega}\text{Im}\left[\frac{\tilde{p}(\omega)}{\tilde{A}(\omega)}\right], \qquad (1)$$

where p is the electron momentum, A is the vector potential of the external field, and the tilde denotes the Fourier transform, $\tilde{f}(\omega) = (2\pi)^{-1/2}\int dt f(t)\exp(-i\omega t)$. For practical reasons, when computing $\sigma(\omega)$, $p(t)$ is split into two parts, p^- and p^+, defined as

$$p^-(t) = \left[1 - \Phi\left(\frac{t-t_1}{\sigma}\right)\right]p(t),$$
$$p^+(t) = \qquad \Phi\left(\frac{t-t_1}{\sigma}\right)\ p(t), \qquad (2)$$

where $\Phi(x)$ is a step function that increases smoothly from 0 to 1 in an interval with characteristic width 1, while t_1 and σ are chosen so that, at any time t for which the external field is non-negligible, $(t_1-t)/\sigma \gg 1$. The p^- term contains the contribution to the dipole during the interaction with the pump and probe pulses, whereas p^+ accounts for the field-free propagation well after the interaction of the atom with the two pulses is over. Since the Fourier transform is linear, p^+ and p^- can be transformed separately and added to get $\tilde{p} = \tilde{p}^- + \tilde{p}^+$. The term $\tilde{p}^-$ has an effectively compact support, comprised between any time t_0 prior the arrival of the external pulses and any time t_2 after the step time window, $(t_2-t_1)/\sigma \gg 1$. Its Fourier transform, therefore, can be easily computed numerically from the tabulated values of $p^-(t)$ in the interval $t \in (t_0, t_2)$.

Since, by construction, the step function approximately equals zero after the end of the field, p^+ is accurately expressed in terms of the field-free evolution of the wave packet spectral components:

$$p^+(t) \approx \Phi\left(\frac{t-t_1}{\sigma}\right)\sum_{i,j}c_i^* c_j\langle j|\hat{P}|i\rangle e^{-i\omega_{ij}t}, \qquad (3)$$

where $\omega_{ij} = \omega_i - \omega_j$, being ω_i the excitation frequency of the eigenstate $|i\rangle$, c_i the corresponding transition amplitude in the interaction representation, obtained from the solution of the TDSE, and $\hat{P}$ is the z-component of the dipole operator. Since the XUV pulse is weak and the VIS is not sufficiently intense to excite the ground state of helium, the majority of the population will remain in the ground state. This entails that, for $i,j > 0$, $1 \simeq |c_0|^2 \gg |c_0^* c_i| \gg |c_i^* c_j|$, and hence only the terms in (3) between the ground state and the $^1P^o$ states give an appreciable contribution to the XUV spectrum of p^+,

$$p^+(t) \approx 2\Phi\left(\frac{t-t_1}{\sigma}\right)\text{Re}\left\{\sum_{\{i|L=1\}}c_i^* c_0\langle 0|\hat{P}|i\rangle e^{-i\omega_i t}\right\}. \qquad (4)$$

In this work, we choose Φ to be the cumulative distribution function, $\Phi(x) = [1 + \text{erf}(x/\sqrt{2})]/2$, in which case $\tilde{p}^+$ can be computed analytically.

To compute $\tilde{p}^-$, it is necessary to evaluate $p(t) = \langle\Psi(t)|\hat{P}|\Psi(t)\rangle$, up to a sufficiently long time after the end of the pulses. The state vector $|\Psi(t)\rangle$ that satisfies the TDSE, with the ground state as initial condition, is obtained from the repeated action of a second-order exponential split operator $U(t+dt,t)$

$$|\Psi(t+dt)\rangle = U(t+dt,t)|\Psi\rangle, \qquad (5)$$
$$U(t+dt,t) = e^{-idtV_{\text{abs}}} \times \qquad (6)$$
$$\times e^{-i\frac{dt}{2}H_0}e^{-idt\alpha A\left(t+\frac{dt}{2}\right)\hat{P}}e^{-i\frac{dt}{2}H_0} \qquad (7)$$

where H_0 is the field-free Hamiltonian, V_{abs} is an absorbing potential that prevents the electron from being reflected at the box boundaries (the radius of the box is 1200 a.u.), α is the fine structure constant, $A(t)$ is the z-component of the external vector potential, and dt the integration time step. In our implementation of the TDSE solver, the state vector is expressed in the basis of eigenfunctions of H_0,

$$|\Psi(t)\rangle = \sum_i |i\rangle c_i(t). \qquad (8)$$

The eigenstates of the field-free Hamiltonian were represented in a basis of radial B-spline functions and bipolar spherical harmonics. Each total angular momentum comprises all the partial-wave channels with configurations $Nl\epsilon_{l'}$ with $N \leq 3$ and $l \leq 11$ and full-CI localized channels $nln'l'$ ($l, l' < 5$) that reproduce short-range correlations between the two electrons. The basis of eigenstates was restricted to states with total angular momentum $L \leq 2$.

In the spectral basis of H_0, the action of the field-free components of the propagator is readily computed,

$$e^{-i\frac{dt}{2}H_0}\sum_i |i\rangle c_i(t) = \sum_i e^{-i\frac{dt}{2}\omega_i}|i\rangle c_i(t). \qquad (9)$$

The field-driven propagation of the state is evaluated using a Krylov method. Finally, the absorbing potential has the form $V_{\text{abs}}(\vec{r}_1, \vec{r}_2) = v(|\vec{r}_1|) + v(|\vec{r}_2|)$, with

$$v(r) = \begin{cases} 0 & , r < r_0, \\ -c_{\text{abs}}(r-r_0)^2 & , r \geq r_0. \end{cases} \qquad (10)$$

For the present simulations, we have used $c_{\text{abs}} = -(1 + 5i) \times 10^{-4}$ a.u., and $r_0 = 1000$ a.u.. At such large values of r_0 the parent-ion wave functions are negligible. The potential, therefore, acts independently on each close-coupling channel, so that the spectral decomposition of V_{abs} is

$$V_{\text{abs}} = \sum_L \sum_n \sum_{i=1} \lambda_i |\phi_{Lni}\rangle\langle\phi_{Lni}| \qquad (11)$$

where L is the total angular momentum, n is the channel index, and λ_i are a single-channel absorption-potential

eigenvalues (the spectrum is the same for all channels), and $|\phi_{L,n,i}\rangle$ the corresponding eigenstates. The majority of the eigenvalues λ_i are zero, so the absorption part of the time-evolution operator can conveniently be written as

$$e^{-idtV_{\mathrm{abs}}} = 1 + \sum_{Ln} \sum_{\{i|\lambda_i \neq 0\}} \left(e^{-idt\lambda_i} - 1\right) |\phi_{Lni}\rangle\langle\phi_{Lni}|. \tag{12}$$

The propagator uses LAPACK [24] and was parallelized using PETSc libraries [25, 26]. All dipole couplings were evaluated in the velocity gauge. The time delay between the pump and probe pulses were varied between -10 fs and 20 fs, and was changed by increments of 3.475 fs.

III. RESULTS AND DISCUSSION

A. Photoionization spectrum

To validate the results of our simulations, we have evaluated the photoionization spectrum above the $N = 2$ threshold, $\sigma_0(\omega)$, and compared it with available experiments [27] and theoretical calculations [28]. The results are shown in Figure 2. Except for a constant upward shift, our results are in excellent agreement with those of Ref. [28] up to a photon energy of around 2.65. In particular, the Fano profiles of the first terms of the well known $[011]_n^+$ dominant series of autoionizing states are well represented. The most prominent resonance can approximately be identified as the $3s3p$ state. In general, however, for DES the independent-particle single-configuration representation is not appropriate, and one should use a classification scheme that accounts for static correlation at the outset. One such scheme makes use of the parabolic notation $[N_1N_2m]_n^A$ where N_1, N_2 and m are the hydrogenic Stark quantum numbers, and $A = \pm 1$ indicates parity under permutation of the radial variables. See [29–34] for a comprehensive list of DES classification schemes. The peaks of the other four $^1P^o$ series converging to the $N = 3$ threshold are too narrow and weak to be observed in the experimental data. In the present calculation, we do not explicitly include the channels above the $N = 3$ ionization threshold, since they are closed in the energy region of interest. The autoionizing states between the $N = 2$ and $N = 3$ thresholds originate from the localized pseudo-channel that describes correlation at short range. Whereas the first couple of terms in each series are well represented, higher terms are not reproduced in the theoretical spectrum. This is not a severe limitation since only the first couple of states in each symmetry, which have the lowest energy and the strongest coupling between each other and the ground state, are anticipated to be responsible for the main features in the spectrum (see also Figure 1).
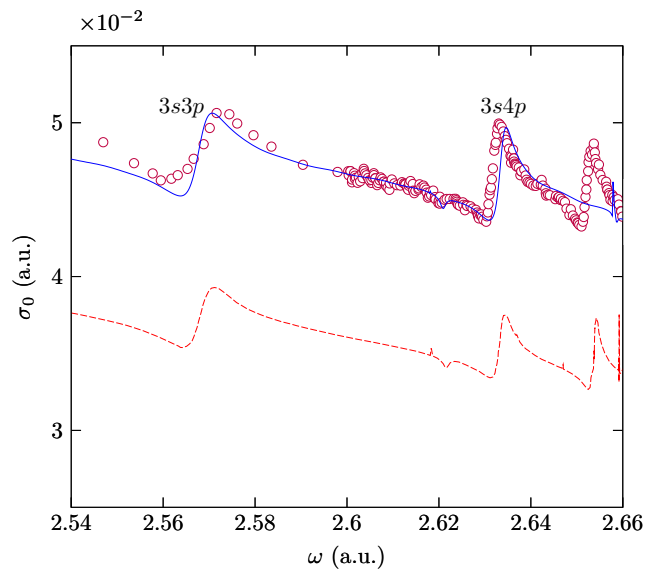

FIG. 2. Photoionization cross section of helium above the $N = 2$ threshold. Full (blue) line: our results. Dashed, red line: theoretical results of Ref. [28]. Circles: experimental results of Ref. [27] renormalized to our theoretical results.

B. Attosecond transient absorption spectrum

Due to the dipole selection rule, the XUV pulse can only populate states of $^1P^o$ symmetry. For this reason, ATAS is mostly sensitive to $^1P^o$ states. In a perturbative perspective, therefore, those processes that involve the exchange of an even number of VIS photons and no net change in angular momentum will preferentially leave a mark in the transient-absorption spectrum. These multiphoton transitions involve resonant excursions through other manifolds, such as $^1S^e$ and $^1D^e$, in such a way that ATAS eventually bears the signature of states with those symmetries as well. In the present calculation, we have limited the eigenstate expansion to total angular momentum $L \leq 2$, so that only states with $^1S^e$, $^1P^o$ and $^1D^e$ symmetries will be observed, i.e., all those states that can be reached by the combination of one XUV and one VIS photon, and most states that can be reached by the combination of one XUV and two VIS photons. Due to the moderate intensity of the VIS pulse used in our calculations, we do not expect that more than two VIS photons are efficiently absorbed/emitted.

Figure 3 shows the calculated attosecond transient absorption spectrum $\sigma(\omega, t_d) = \sigma(\omega)\big|_{t_d}$ as a function of the XUV-VIS time delay and the photon energy of the transmitted XUV light. Negative time delays correspond to the control pulse arriving before the XUV pulse. The vertical features are due to the bright $3snp$ series of DES, $n = 3, 4$ also seen in Figure 2. At large negative time delays the spectrum is identical to the field-free photoionization spectrum shown in Figure 2, σ_0. For positive large delays, on the other hand, the VIS pulse does alter the excited states that have been populated by the

XUV pulse, leading to the appearance of more involved structures and fringes around the resonant peaks. When the two pulses overlap, the $3s3p$ $^1P^o$ peak splits into AT branches as a result of the resonant coupling of this state with the $3s4s$ $^1S^e$ and $3d^2$ $^1D^e$ states through absorption of a single VIS photon (higher nearby states also contribute to the splitting although to a lesser extent). The latter two states are "dark" in single-photon ionization from the ground state, since they are forbidden by the dipole selection rule. While the VIS pulse is traversing the target, however, both the ground and the doubly-excited states with even parity are dressed by the VIS field. As a result, they acquire an instantaneous $^1P^o$ component. Radiative transitions between such dressed states, therefore, become possible. Indeed, faint signatures of these transitions are visible when the XUV and VIS pulses overlap. Below the $N = 2$ threshold, the strong coupling between the sp_2^+ $^1P^o$ and the $2s^2$ $^1S^e$ states gives rise, even at comparatively low intensities, to a well recognizable AT doublet. Only at larger intensities is the subsequent sp_3^+ involved in the Rabi oscillation, and the resonant peaks split further [2]. Due to the larger number of dark states taking part in the present study, the AT splittings are more involved at the outset.

As the time delay increases, the transient-absorption spectrum, $\sigma(\omega, t_d)$, approaches σ_0,

$$\lim_{t_d \to \infty} \sigma(\omega, t_d) \to \sigma_0(\omega). \qquad (13)$$

In this time region, the slowly varying fringes converging around each resonance are the result of the sharp change in the phase and population of the localized part of the resonances induced by the strong VIS pulse [16]. In Figure 3, the most prominent asymptotes are at 2.57 and 2.64. These features are qualitatively similar to those observed in ATAS of He below the $N = 2$ threshold [2] or of H_2 below the ionization threshold [35] (see the latter reference for a more detailed analysis).

The densely packed transversal hyperbolic fringes appearing on top of the $3s3p$ and $3s4p$ resonances have a different origin. They approximately follow the formula $\tau_k(\omega) = 2\pi k/|\omega - \omega_{3snp}|$ and arise from the interference between the direct one-photon excitation amplitude from the ground state and a resonantly enhanced n-VIS-photon emission and absorption amplitude from the other XUV-excited autoionizing states or the continuum. These fringes are more apparent in Figure 3 for $t_d > 5$ fs. The specific states involved in these transitions are more clearly identified by performing the bidimensional analysis of ATAS described in the following section.

C. Bidimensional Spectroscopy

The XUV pulse used for the present work is comparatively weak. Any observable, therefore, can be accurately expanded in a perturbative series of either $\mathcal{E}_{\mathrm{XUV}}(t)$ or
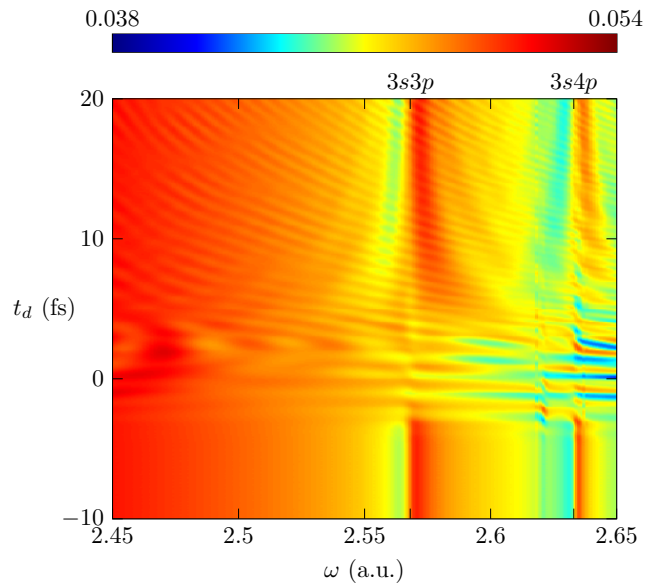

FIG. 3. The attosecond transient absorption spectrum of helium above the $N = 2$ ionization threshold. The abscissa shows the response energy and the ordinate shows the time delay t_d between the pulses.

$\tilde{\mathcal{E}}_{\mathrm{XUV}}(\omega)$, the z component of the XUV field and spectrum, respectively, truncated to lowest order. In particular, after exciting the atom, the XUV pulse does not induce any significant population transfer between, or phase change of, excited states. This means that, in absence of a control pulse, if the atom is excited to a state with energy $\hbar\omega_e$ above the ground state, it will respond in the XUV spectrum at the same frequency $\omega_r = \omega_e$. The VIS pulse, however, can transfer population between an excited state with energy ω_e to one with energy ω_r, in such a way that the atomic dipole can oscillate at a response frequency $\omega_r \neq \omega_e$.

It is possible to observe the effect of the VIS pulse on the response frequencies ω_r, as a function of the excitation frequency ω_e, from the Fourier transform of $\sigma(\omega, t_d)$. The transient-absorption spectrum, of course, is dominated by the constant asymptotic background σ_0 at $t \to \pm\infty$, whose Fourier transform is trivial, and which therefore can be removed at the outset. We thus define [2]

$$\tilde{\sigma}(\omega_r, \omega_t) = \int dt_d \left[\sigma(\omega_r, t_d) - \sigma_0(\omega_r) \right] \frac{e^{-i\omega_t t_d}}{\sqrt{2\pi}}. \qquad (14)$$

The function $\tilde{\sigma}(\omega_r, \omega_t)$ is related to the non-diagonal elements $\chi_{\mathrm{nd}}(\omega_r, \omega_e)$ of the electric susceptibility of the dressed atom [2] through the formula

$$\tilde{\sigma}(\omega_r, \omega_t) \propto \left[\chi_{\mathrm{nd}}(\omega_r, \omega_r - \omega_t) - \chi_{\mathrm{nd}}^*(\omega_r, \omega_r + \omega_t) \right]. \qquad (15)$$

Figure 4(a) shows the absolute value of $\tilde{\sigma}(\omega_r, \omega_e - \omega_r)$, on a logarithmic scale, as a function of ω_r and ω_e. To evaluate the Fourier transform (14), we would need the transient-absorption spectrum at arbitrarily large time
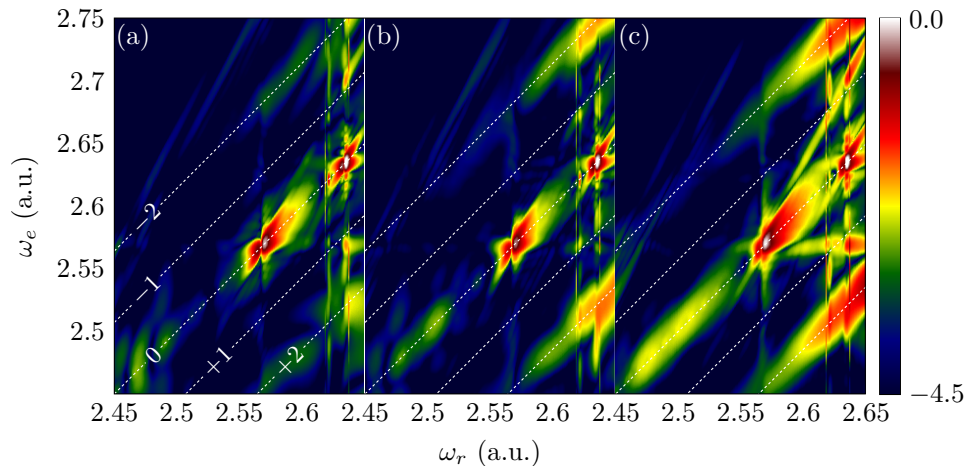
FIG. 4. In (a), the natural logarithm of the absolute value of the bidimensional absorption spectrum, $\ln |\tilde{\sigma}(\omega_e, \omega_r - \omega_e)|$, above the $N = 2$ threshold of Helium. The abscissa shows the electron response energy ω_r, and the ordinate shows the excitation energy ω_e. The diagonal, dashed lines are separated by ω_{VIS}. Their labels correspond to the number of absorbed (positive) and emitted (negative) VIS photons. In (b) and (c), similar plots are shown for two artificial cases. In (b), the $^1S^e$ states, excluding the ground state, are artificially removed. In (c), the $^1D^e$ states are removed.

delays. Here, we switch off the spectrum, near the upper limit of our time-delay interval, with a smooth step function prior to carrying out the Fourier transform. This procedure limits the resolution of the spectrum along the ω_e axis, but the main features are still visible, and reasonably well resolved in the case of the resonances whose lifetime is smaller than our maximum time delay. The net exchange of n VIS photons from a state with excitation frequency ω_e will cause a response at $\omega_e = \omega_r \pm n\omega_{\mathrm{VIS}}$. Figure 4 shows dashed lines demarcating the regions corresponding to these possible transitions. All the peaks in $\tilde{\sigma}(\omega_r, \omega_r - \omega_e)$ resulting from the interaction with the VIS pulse are expected to appear on top of these lines. Indeed, this is what is seen for most structures in Figure 4(a). The most prominent peaks are found at excitation energies of 2.57 and 2.45, along the $\omega_r = \omega_e$ diagonal, and at $\omega_r = 2.45$ along the $\omega_r = \omega_e - 2\omega_{\mathrm{VIS}}$ line. These structures are the signature of a two-photon beating between the $3s3p\ ^1P^o$ DES and a non resonant $^1P^o$ continuum state at $\omega_e \approx 2.45$, indicating the formation of a correlated two electron wave packet resulting from the coherent superposition of these states.

One can also see the signature of the $3s4p\ ^1P^o$ DES located at $\omega_e \approx 2.64$ along the $\omega_r = \omega_e$ diagonal, as well as a structure at around (2.64,2.52) on the $\omega_r = \omega_e - 2\omega_{\mathrm{VIS}}$ line, which is due to two-photon beatings between this state and the non resonant continuum states of the same symmetries lying at $\omega_e \simeq 2.52$. These beatings are mediated by a resonant one-photon transition to lower $3l3l'$ DES of $^1S^e$ and $^1D^e$ symmetries. There is another pronounced structure at around (2.64,2.75), which is due to two-photon beatings between the $3s4p\ ^1P^o$ DES with higher $^1P^o$ DES ($\omega_r = 2.77$). Finally, the peaks at (2.64,2.57) and (2.64,2.70) could be due to a combination of the following processes: (i) one-photon beatings

between the $3s4p\ ^1P^o$ state and lower $3l3l'\ ^1S^e$ and $^1D^e$ DES, in particular, the $3s^2\ ^1S^e$ one, which is dipole-allowed in an independent electron picture (i.e., it does not require electron correlation), (ii) one-photon beatings between the $3s3p\ ^1P^o$ state and higher $3l3l'\ ^1S^e$ and $^1D^e$ DES, in particular, the $3s4s\ ^1S^e$ one, which is also-dipole allowed in an independent electron picture, and (iii) one-photon beatings between the dressed $3s3p$ and $3s4p\ ^1P^o$ states. These are in fact different sides of the same process: the dressing of the $^1P^o$ DES by the IR field through one-photon transitions, so they cannot be disentangled. Higher order n-photon beatings are not observed in the bidimensional spectrum. Some of the transitions involving the $3s3p\ ^1P^o$ and $3s4p\ ^1P^o$ DES are schematically represented in Figure 1.

To assign the peaks in the $\tilde{\sigma}(\omega_r, \omega_e - \omega_r)$ spectrum one has to take into account that the VIS pulse promotes transitions between states that satisfy the resonant condition $\Delta\omega = n\omega_{\mathrm{VIS}}$ when their energies include the AC-Stark shift. The XUV transition from and to the ground state, however, may take place in absence of the dressing pulse. The off-diagonal peaks in the bidimensional spectrum, therefore, are also shifted from the reference $\omega_r = \omega_e + n\omega_{\mathrm{VIS}}$ line by an amount comparable to the difference between the AC-Stark shifts of the states involved [2, 36–38]. This effect can be seen for the maxima in the neighborhood of (2.64,2.57) and (2.64,2.70) in Figure 4(a), which are clearly displaced with respect to their expected positions.

To gain deeper insight on the origin of the different structures observed in the bidimensional spectrum, we show in Figures 4(b) and (c) the results of two artificial ATAS simulations in which the $^1S^e$ states (except for the ground state) and the $^1D^e$ states have been excluded, respectively. After removing the $^1S^e$ states, the

main difference to the full spectrum is the significant decrease of the (2.64,2.57) and (2.64,2.70) peaks, confirming that the majority of the one-photon beatings involving the $3s3p$ and $3s4p$ $^1P^o$ states ($\omega_e \approx 2.57$ and 2.64) occur with states of $^1S^e$ symmetry, in particular the $3s4s$ and $3s^2$ $^1S^e$ ones, respectively, rather than with states of $^1D^e$ symmetry (see Figure 1). This interpretation is confirmed by the bidimensional spectrum obtained by excluding the $^1D^e$ states, where the corresponding peaks are even more pronounced than in the full spectrum. All other structures (beatings) discussed above remain visible in the artificial bidimensional spectra, indicating that states of both $^1S^e$ and $^1D^e$ symmetries contribute significantly to the observed beatings.

IV. CONCLUSIONS

In this paper we have theoretically investigated ATAS of Helium above the $N = 2$ ionization threshold, where several ionization channels are open. By using XUV pump and VIS control pulses similar to those employed in recent experiments [4], we are able to induce sizable resonant one-photon transitions between the $3snp$ $^1P^o$ doubly excited states and the $3l3l'$ $^1S^e$ and $^1D^e$ states. More interestingly, two-photon beatings associated with the bound-continuum transition from the $3s3p$ $^1P^o$ doubly excited state to the non resonant $^1P^o$ multichannel continuum lying just above $N = 2$ are also observed, thus leading to the formation of a multichannel two-electron correlated wave packet. Both effects lead to a significant distortion of the $3snp$ Fano profiles and to a strong variation of these profiles with the pump-probe delay. Hence, as for resonances lying below the $N = 2$ threshold, control of the multi-channel two-electron correlated wave packet generated by this combination of pulses is

possible.

As multichannel ionization continua are more the rule than the exception in most atomic systems and in all molecules, the present results show that the additional complications brought by the opening of several channels should not pose major challenges for the applicability of ATAS to these systems. At most, as shown in the present work, one might expect a more prominent role of two-photon beatings between quasi-bound resonant states and non resonant continuum states, which have not hitherto been observed in previous single-channel ATAS experiments. The main limitation, however, would be that some of the observed structures might not be unambiguously attributed to a specific process but to a combination of several ones. Although disentangling the individual contributions in these special cases is not possible by using the standard ATAS approach discussed in the present work, such limitation could be overcome by using two independent IR pulses: one to dress the atom at the time of the XUV transition, and the other one to promote the transitions between the different states. This is standard practice in femtosecond pump-probe spectroscopy, and should not be difficult to implement in current ATAS experiments.

V. ACKNOWLEDGMENTS

[1] C. Ott, A. Kaldun, L. Argenti, P. Raith, K. Meyer, M. Laux, Y. Zhang, A. Blttermann, S. Hagstotz, T. Ding, R. Heck, J. Madroñero, F. Martín, and T. Pfeifer, Nature **516**, 374 (2014).

[2] L. Argenti, Á. Jiménez-Galán, C. Marante, C. Ott, T. Pfeifer, and F. Martín, Physical Review A **91** (2015), 10.1103/physreva.91.061403.

[3] E. Goulielmakis, Z.-H. Loh, A. Wirth, R. Santra, N. Rohringer, V. S. Yakovlev, S. Zherebtsov, T. Pfeifer, A. M. Azzeer, M. F. Kling, S. R. Leone, and F. Krausz, Nature **466**, 739 (2010).

[4] C. Ott, A. Kaldun, L. Argenti, P. Raith, K. Meyer, M. Laux, Y. Zhang, A. Blättermann, S. Hagstotz, T. Ding, R. Heck, J. Madroñero, F. Martín, and T. Pfeifer, Nature **516**, 374 (2014).

[5] A. R. Beck, B. Bernhardt, E. R. Warrick, M. Wu, S. Chen, M. B. Gaarde, K. J. Schafer, D. M. Neumark, and S. R. Leone, New J. Phys. **16**, 113016 (2014).

[6] E. Heinrich-Josties, S. Pabst, and R. Santra, Phys. Rev. A **89**, 043415 (2014).

[7] A. Wirth, M. T. Hassan, I. Grguras, J. Gagnon, A. Moulet, T. T. Luu, S. Pabst, R. Santra, Z. a. Alahmed, A. M. Azzeer, V. S. Yakovlev, V. Pervak, F. Krausz, and E. Goulielmakis, Science **334**, 195 (2011).

[8] X. Wang, M. Chini, Y. Cheng, Y. Wu, X.-m. Tong, and Z. Chang, Phys. Rev. A **87**, 063413 (2013).

[9] S. Chen, M. J. Bell, A. R. Beck, H. Mashiko, M. Wu, A. N. Pfeiffer, M. B. Gaarde, D. M. Neumark, S. R. Leone, and K. J. Schafer, Phys. Rev. A **86**, 063408 (2012).

[10] S. Chen, M. Wu, M. B. Gaarde, and K. J. Schafer, Phys. Rev. A **87**, 033408 (2012).

[11] S. Chen, M. Wu, M. B. Gaarde, and K. J. Schafer, Phys. Rev. A **88**, 033409 (2013).

[12] J. Herrmann, M. Weger, R. Locher, M. Sabbar, P. Rivière, U. Saalmann, J.-M. Rost, L. Gallmann, and U. Keller, Phys. Rev. A **88**, 043843 (2013).

[13] M. Chini, X. Wang, Y. Cheng, and Z. Chang, J. Phys. B: At. Mol. Opt. Phys. **47**, 124009 (2014).

[14] J. Ullrich, R. Moshammer, A. Dorn, R. Dörner, L. P. H. Schmidt, and H. Schmidt-Böcking, Rep. Prog. Phys. **66**, 1463 (2003).

[15] A. T. J. B. Eppink and D. H. Parker, Rev. Sci. Instrum. **68**, 3477 (1997).

[16] A. Kaldun, A. Blättermann, V. Stooß, S. Donsa, H. Wei, R. Pazourek, S. Nagele, C. Ott, C. D. Lin, J. Burgdörfer, and T. Pfeifer, Science **354**, 738 (2016), http://science.sciencemag.org/content/354/6313/738.full.pdf.

[17] C. Ott, A. Kaldun, P. Raith, K. Meyer, M. Laux, J. Evers, C. H. Keitel, C. H. Greene, and T. Pfeifer, Science **340**, 716 (2013).

[18] A. Blättermann, C. Ott, A. Kaldun, T. Ding, and T. Pfeifer, J. Phys. B: At. Mol. Opt. Phys. **47**, 124008 (2014).

[19] A. Kaldun, C. Ott, A. Blättermann, M. Laux, K. Meyer, T. Ding, A. Fischer, and T. Pfeifer, Phys. Rev. Lett. **112**, 103001 (2014).

[20] A. Burgers, D. Wintgen, and J. M. Rest, Journal of Physics B: Atomic, Molecular and Optical Physics **28**, 3163 (1995).

[21] J. M. Rost, K. Schulz, M. Domke, and G. Kaindl, Journal of Physics B: Atomic, Molecular and Optical Physics **30**, 4663 (1997).

[22] M.-K. Chen, Physical Review A **56**, 4537 (1997).

[23] J. M. Rost, K. Schulz, M. Domke, and G. Kaindl, Journal of Physics B: Atomic, Molecular and Optical Physics **30**, 4663 (1997).

[24] E. Anderson, Z. Bai, C. Bischof, S. Blackford, J. Demmel, J. Dongarra, J. Du Croz, A. Greenbaum, S. Hammarling, A. McKenney, and D. Sorensen, *LAPACK Users' Guide*, 3rd ed. (Society for Industrial and Applied Mathematics, Philadelphia, PA, 1999).

[25] S. Balay, S. Abhyankar, M. F. Adams, J. Brown, P. Brune, K. Buschelman, V. Eijkhout, W. D. Gropp, D. Kaushik, M. G. Knepley, L. C. McInnes, K. Rupp, B. F. Smith, and H. Zhang, *PETSc Users Manual*, Tech. Rep. ANL-95/11 - Revision 3.5 (Argonne National Laboratory, 2014).

[26] S. Balay, W. D. Gropp, L. C. McInnes, and B. F. Smith, in *Modern Software Tools in Scientific Computing*, edited by E. Arge, A. M. Bruaset, and H. P. Langtangen (Birkhäuser Press, 1997) pp. 163–202.

[27] A. Menzel, S. P. Frigo, S. B. Whitfield, C. D. Caldwell, and M. O. Krause, Physical Review A **54**, 2080 (1996).

[28] R. Moccia and P. Spizzo, Physical Review A **43**, 2199 (1991).

[29] G. Tanner, K. Richter, and J. M. Rost, Rev. Mod. Phys **72**, 497 (2000).

[30] C. D. Lin, Adv. At. Mol. Phys. **22**, 77 (1986).

[31] C. D. Lin, Phys. Rev. A **29**, 1019 (1984).

[32] D. R. Herrick, M. E. Kellman, and R. D. Poliak, Phys. Rev. A **22**, 1517 (1980).

[33] J. M. Feagin and J. S. Briggs, Phys. Rev. Lett. **57**, 984 (1986).

[34] D. R. Herrick and O. Sinanoğlu, Phys. Rev. A **11**, 97 (1975).

[35] Y. Cheng, M. Chini, X. Wang, A. González-Castrillo, A. Palacios, L. Argenti, F. Martín, and Z. Chang, Phys. Rev. A **94**, 023403 (2016).

[36] R. R. Freeman, N. P. Economou, G. C. Bjorklund, and K. T. Lu, Physical Review Letters **41**, 1463 (1978).

[37] R. R. Freeman, P. H. Bucksbaum, H. Milchberg, S. Darack, D. Schumacher, and M. E. Geusic, Physical Review Letters **59**, 1092 (1987).

[38] R. Freeman and P. Bucksbaum, Journal of Physics B: Atomic, Molecular and Optical Physics **24**, 325 (1991).